Nucleation and growth of metallic submonolayers on compact metal surfaces

P. Blandin and C. Massobrio
Institut de Physique Expérimentale, Ecole Polytechnique Fédérale de Lausanne, PHB Ecublens, CH 1015 Lausanne, Switzerland

P. Ballone
Institut für Festkörperforschung, Forschungszentrum Jülich, D-52425 Jülich, Germany
(Received 5 November 1993)

By use of the molecular-dynamics method we study the high-temperature nonequilibrium and equilibrium properties of a metallic overlayer on a compact metal surface. The system is modeled by the embedded-atom method, and consists of a Pt slab with a large ideal (111) surface (cross section of 930 atoms) on which Ag atoms are randomly distributed with coverages $\Theta=0.10$, 0.25, 0.30. We simulate the short-time ($\tau\sim 1$ ns) process by which the adatoms form dynamically stable aggregates in local equilibrium with a dilute two-dimensional vapor. We analyze the equilibrium properties of the adlayer as a function of T and Θ. We compute the cluster size distribution, the adatom radial-distribution function, the diffusion coefficient, and we characterize the cluster shape by the ratio of its principal moments of inertia. At all Θ and T the Ag islands grow pseudomorphically on Pt(111). At high temperatures ($T\sim 1000$ K) the clusters are fluidlike. There is no evidence of peculiar stability at the sizes corresponding to the filling of two-dimensional close-packing shells ("magic numbers," $N=7$, 10, etc.). At intermediate temperatures ($T=600$–800 K) the size distribution is shifted toward larger aggregates and, at low coverage, starts to display stability peaks at the magic numbers. The larger clusters develop a solidlike core surrounded by a fluidlike boundary. At the lowest temperature of our study ($T=400$ K) the clusters display a high degree of local order. The size distribution function is restricted to small N's by the slowing down of the cluster growth beyond the nucleation stage. At $\Theta=0.10$ the stability peaks at $N=7$ and 10 are apparent. We discuss the influence of a step on the behavior of the system.

I. INTRODUCTION

Recent years have witnessed a rapid growth of experimental and theoretical investigations of metal overlayers on solid surfaces.[1] Of primary interest have been metal overlayers on semiconductors, because of their relevance for electronic devices.[2] A large number of studies, however, have also been devoted to metal overlayers on metal surfaces, that are the subject of the present paper. The interest in these systems is motivated by their role as simple and well-characterized models for two-dimensional (2D) ordering and for crystal growth, as well as by their potential for applications.

In what follows, our main interest will be in the kinetics and thermodynamics of the early stages of film growth, and, therefore, we will focus on submonolayer coverages. Metal overlayers in this coverage range are produced by physical (evaporation, molecular-beam epitaxy, sputtering) or chemical (metal organic vapor deposition, pyrolysis) means.[3] The deposition process and the resulting film are monitored and analyzed by a variety of experimental techniques, including diffraction, spectroscopy, and microscopy.[4]

Until now, a larger share of these studies has been devoted to metal overlayers on relatively open surfaces, like the (110) of the fcc metals, or the (111) of the bcc. Open surfaces usually provide specific adsorption sites, separated by large energy barriers limiting the diffusion of the adsorbates. Lattice-gas models are particularly suitable to describe these systems, and have been widely exploited in the past[5] [see also Ref. 6 for representative examples of molecular-dynamics (MD) studies of continuum models].

Less, but growing attention has been devoted to compact substrate surfaces, like the (111) of fcc metals, or the (110) of the bcc. On the one hand, these surfaces present only a limited set of intriguing reconstructions and phase transformations. On the other hand, however, their almost inert behavior implies a stable and easily reproducible substrate for the overlayer deposition and growth. Moreover, compact surfaces usually present very low in plane diffusion barriers. This is particularly true in the presence of metal overlayers, which, by lacking directional bonding and preferential adsorption sites, behave like almost (2D) systems of highly mobile atoms.

These features point to metal overlayers on compact metal surfaces as the ideal prototype to investigate the kinetics of the overlayer assembly upon deposition, and to study the equilibrium properties of the resulting 2D phases on an almost flat substrate. On the theoretical side, lattice-gas models are no longer adequate for these systems, and a quantitative description has to take into account the high atomic mobility and the resulting large entropic contribution.

Elementary thermodynamics suggests that the homogeneous deposition of metal atoms on a flat surface at moderate coverage and T is likely to give rise to an inhomogeneous system by nucleating islands of the condensed phase surrounded by a dilute vapor of adatoms.[7,8] Depending on the relative value of the surface tension of the

substrate and adsorbate, on the interfacial tension, and on temperature, the islands can be 2D (i.e., one monolayer thick) or 3D structures, with the additional possibility of a partial 2D growth *and* the occasional formation of 3D structures.[9]

Besides this qualitative picture, very little quantitative information is available on the coexistence curve of the vapor and the condensate, the size distribution of the islands as a function of T and coverage Θ, the equilibrium phase (either solidlike or liquidlike) of the islands, and the influence of the substrate corrugation on the structure of the adsorbate.

Quantitative information is even less abundant on the dynamics of the adlayer formation. Most of the previous theoretical studies resort to phenomenological rate equations,[10] based on a detailed balance between the different cluster sizes. This approach requires in input several kinetic constants whose values, however, are rather uncertain. The accepted classification[11] subdivides the adlayer organization into three stages: (i) the initial formation of adclusters by either nucleation (involving a free energy barrier) or spinodal decomposition (without barrier); (ii) an early stage growth, in which the condensed nuclei rapidly growth by subtracting atoms from the supersaturated vapor. This stage produces a population of islands in local equilibrium with the vapor; (iii) a late stage evolution, in which the islands grow by coalescence (direct island-island interaction) and ripening (long-range island-island equilibration via the vapor).

In the present study, we select Ag on the ideal Pt (111) surface as a representative example of metal adlayer on a compact metal surface. Experimental information for this system is abundant, starting from the low-energy-electron-diffraction LEED measurements of Ref. 12, and including detailed results from photoemission spectroscopy,[13] helium diffraction,[14] LEED and x-ray-photoemission spectroscopy,[15] and scanning tunnelling microscopy.[16]

The following experimental results provide the basis for our modelization.

(i) The Pt (111) surface is stable up to $T \sim 1300$ K, temperature at which this surface reconstructs.[17]

(ii) This surface, carefully prepared, presents large, almost ideal terraces limited by steps. At moderate temperature, the terrace width can exceed 1000 Å, as can be appreciated in STM (Ref. 18) or reflection electron microscopy (Ref. 19) images.

(iii) Ag on Pt(111) is known to grow layer by layer,[12,13] and, at moderate temperatures, the growth is pseudomorphic.[14,15]

(iv) Up to high temperature, very limited mixing is observed between the Ag and the Pt atoms on terraces.[13] Mixing, however, could occur at steps.[16]

(v) The temperature of thermal desorption is very high [$T \sim 1000$ K for $\theta \leq 1$ (Ref. 15)], and, therefore, this process does not affect the behavior of the system on the time scale of our simulation.

In our study, the Ag/Pt(111) system is modeled by the embedded-atom method (EAM), that, although semiempirical, is very reliable for elements (like Ag and Pt) at the end of the transition series.

We apply molecular dynamics to simulate the first two stages of the adlayer equilibration after deposition from the vapor or from the beam. We consider systems in the temperature range $400 \leq T \leq 1000$ K, and Ag coverages $0.1 \leq \Theta \leq 0.30$. We observe the first aggregation of Ag clusters to occur by spinodal decomposition over a time of the order of 10 psec. Over a longer time scale (~ 1 nsec at $T = 1000$ K, and dependent on temperature) the early stage growth of the condensed nuclei takes place, and we observe a stationary population of islands in local equilibrium with the vapor. The simplicity of the model allows us to continue the simulation well beyond this stage, at least for temperatures in excess of ~ 600 K. We characterize the island population during this long-time, long-distance equilibration stage in terms of their size distribution, the ratio of the principal moments of inertia, and diffusion properties. We also determine the coexistence curve for the vapor of adatoms and dimers in equilibrium with the condensed islands.

At moderate T and Θ we observe weak peaks in the size distribution corresponding to compact, highly coordinated clusters. At temperatures of the order of ~ 800 K the peaks disappear, and the size distribution becomes smooth.

A detailed analysis of atomic configurations and dynamical properties shows that the thermodynamic "state" of the islands can be classified into the following three categories.

(i) At low T ($T < 600$ K) the islands are characterized by a well-defined local atomic order. At variance with a truly solid system, however, the islands can easily change their shape.

(ii) At intermediate T and for large islands ($N > 20$) it is possible to recognize a solidlike core of the cluster, surrounded by a fluid boundary.

(iii) At higher T the local atomic order is completely lost, and the islands are liquidlike.

To complete our analysis we performed few simulations at higher coverages ($\Theta = 0.30$, 0.75). At $\Theta = 0.30$ and $T = 1000$ K we observe the onset of island percolation across the system. The long time and length scale of this process, however, prevents a detailed description by MD.

The $\Theta = 0.75$ coverage is the complementary of $\Theta = 0.25$ under interchange of the adatoms with the advacancies (i.e., atoms missing to complete the layer), and we simulated this system to investigate whether there is some degree of symmetry between the early and late stages of the adlayer formation. We find that at high T the advacancy is not well defined, and the symmetry does not hold. At lower T the advacancy is progressively better defined, and it is possible to recognize some elements of symmetry. The correspondence, however, is never very good.

Finally, we simulate the system in the presence of a straight step on the (111) Pt surface. We observe that the step gives rise to an attractive potential extending over several interatomic distances into the lower terrace. The adsorbate is progressively confined by this potential that acts as a sink of adatoms and adclusters. The upper terrace of the step appears to be much less perturbed.

II. THE MODEL AND THE SIMULATION METHOD

To model a wide metal surface, a large number of metal atoms adsorbed on it, and to follow the system during the long time needed to reach local equilibrium, we resort to the well known embedded-atom method.[20] This scheme, introduced ten years ago by Daw and Baskes,[21] has been successfully applied to study a variety of properties of bulk transition metals and alloys.[22,23] It has also been extensively exploited to study surfaces and interfaces.[24] Despite several quantitative problems (the most important of which is a severe underestimation of surface energies, at least in the original formulation of the scheme), it has achieved a remarkable degree of success in describing surface geometries, relaxations, and reconstructions. A recent study has shown that it reliably describes the energetics of surface defects like steps and kinks.[25] Finally, EAM has been used by two of us to study several properties of metal clusters on surfaces, including static configurations, diffusion, and cluster-surface collisions.[26]

Despite several refinements have already been proposed in the literature,[27] we apply the original formulation of the EAM method because of its simplicity and of its extensive record of reliability. The parametrization we use to model transition metal mixtures is that of Ref. 23.

Our system consists of a Pt slab (12 layers) with a wide (111) ideal surface (930 atoms per plane) with periodic boundary conditions in two dimensions. To fix the notation, we choose the z axis perpendicular to the surface. After full relaxation, the surface energy of the slab turns out to be $\sigma = 1440$ ergs/cm^2, to be compared with the experimental estimate of ~ 2000 ergs/cm^2 (Ref. 28). Over this substrate, an overlayer of Ag atoms is deposited, with increasing coverage in the submonolayer range.

The accuracy of the EAM description for these systems rests on the fact that the adsorbed atoms always are embedded in a metallic environment. The validity of this assumption is best demonstrated by photoemission measurements of Ag/Pt(111) [13] showing that three Ag layers already display an almost bulklike band structure, that starts to develop at the lowest detectable coverage.

The static properties of a metal adatom on this surface have been studied in Ref. 26. The equilibrium position of the adatom is the C site (see Fig. 1 of Ref. 26 for a schematic drawing of the surface geometry and the definition of the A, B, and C sites), with an adsorption energy of -2.72 eV. The A site is only 0.005 eV higher in energy (i.e., at the same energy within the accuracy of the computation). The static diffusion barrier E_0 between two C sites is 0.05 eV. Little direct comparison is available for E_0 from experiments on Ag/Pt(111). Experimental data for similar systems [$E_0 = 0.065$ eV for Ag/Ag(111),[29] 0.040 eV for Au/Au(111) (Ref. 30)], however, suggest that the EAM value for E_0 is realistic. Very recent experimental estimates suggest a barrier $E_0 = 0.15$ eV (Ref. 31). Even this larger value would be consistent with fast diffusion of the adatoms at the temperatures of the present study, and, therefore, would not invalidate our conclusions.

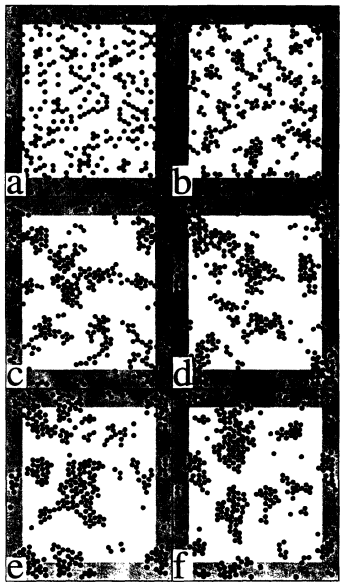

FIG. 1. Snapshots of the adatom configurations, $\Theta = 0.25$, $T = 1000$ K. (a) Starting (random) distribution; (b) $t = \tau_N = 5.6$ psec after deposition; (c) $t = 0.8$ nsec; (d) $t = 1.6$ nsec; (e) $t = 2.4$ nsec; (f) $t = 3.8$ nsec. The shaded area belongs to the periodic replicas of the central region.

The very small lateral corrugation of the potential-energy surface implies a weak coupling of the adatom with the surface via lateral atom displacements, and a fast diffusion for adatoms on the ideal surface. The diffusion coefficient for an Ag adatom at $T = 311$ K, computed in Ref. 26, is $D = 2.4 \times 10^{-5}$ cm^2/sec, and is comparable to that for a good liquid.

We exploit this observation to introduce a drastic simplification: in the following we freeze the Pt surface in a fixed (relaxed) configuration, and we follow the dynamics of the Ag atoms only. This approximation is also justified by the rigid behavior of the Pt substrate (that reconstructs only at $T \sim 1300$ K), and by the experimental observation that there is only very little AgPt intermixing at (111) terraces.[12]

The many body character of the EAM potential imposes some caution in isolating the Hamiltonian H_{ad} for the adlayer. The electron density in which the Ag atoms are embedded contains a contribution from the fixed Pt configuration. Moreover, we retain in H_{ad} the variation of the embedding energy of Pt due to the (time dependent) electron distribution of Ag. Both these effects provide a potential modulation with the periodicity of the (111) surface, in addition to the "external" potential representing the repulsive two-body AgPt interaction.

The frozen substrate approximation greatly reduces the computer time, and significantly extends the reach of our simulation. It has two obvious consequences on the system dynamics: First, it slightly increases the static diffusion barrier for adatoms (now $E_0 = 0.1$ eV, i.e., intermediate between the low and high experimental estimates). Moreover, the decoupling of the adsorbate dynamics from the substrate hampers the in-plane equilibra-

tion of the Ag atoms. The problem is particularly important for isolated adatoms or small aggregates, while it is less severe for large aggregates and high coverage, where the adatom-adatom interaction provides a sufficient thermal bath.

To overcome this last problem, we resort to the Langevin dynamics:

$$M_{\mathrm{Ag}}\ddot{\mathbf{R}}_i = -\gamma\dot{\mathbf{R}}_i - \nabla_i E_c + \mathbf{F}_W \ , \tag{1}$$

where $\mathbf{F}_W$ is a white spectrum random force

$$\langle \mathbf{F}_W(t)\mathbf{F}_W(t')\rangle = 2\gamma K_B T\delta(t-t') \tag{2}$$

and γ is a small friction coefficient ($\gamma \sim 3.4\times10^{-8}$ erg/cm^2).[32] By this choice we ensure the system equilibration, while, at the same time perturbing only slightly the dynamics of the system. A first test has been done by recomputing the diffusion coefficient, that, at $T=600$ K, turns out to be $D=1.3\times10^{-5}$ cm^2/sec, i.e., of the same order of magnitude of the value obtained for the microcanonic dynamics of the entire (substrate+adsorbate) system.[33]

The equations of motion are integrated by a standard velocity Verlet algorithm,[34] with a time step of 1.4×10^{-15} sec.

During the simulation, snapshots of the adatom configuration are plotted at regular intervals of simulation time to provide a direct representation of the system evolution.[35]

Besides this pictorial information, several other quantities are computed to monitor in a quantitative way the approach of the system to equilibrium, and to characterize the resulting phases of the adsorbed layer. First of all, we compute the one body density $\rho(x,y)$ (integrated over the perpendicular direction z), to characterize and quantify the degree of epitaxy in the Ag/Pt(111) growth. Then, we analyze the progressive organization of the adatoms into surface clusters. In what follows, clusters are defined as a connected aggregates of adatoms, in which each of the atoms has at least a neighbor within a cutoff distance R_c equal to 3.5 Å.

The cluster distribution is characterized by the probability function $P(N)$, giving the relative number of clusters of size N over the total number of clusters in the system (including single adatoms). We shall use also the derived distribution $p(N)$, giving the probability for an atom to belong to a cluster of size N. Obviously, $p(N)\propto NP(N)$.

To characterize the cluster shape, we compute the moments of inertia with respect to the principal axes (we consider the x and y dimensions only), and we collect the average of the ratio r between the smaller and the larger of the two moments: $r=I_{\min}/I_{\max}$. A globular aggregate will be characterized by $r\sim1.0$, while a highly anisotropic cluster will present a reduced r. The time fluctuation of r will provide information on the isomerization rate of the clusters.

The atomic configuration within a cluster is monitored via the pair distribution function $g(\mathbf{r}_1,\mathbf{r}_1+\mathbf{r})$, defined, in two dimensions, as

$$g(\mathbf{r}_1,\mathbf{r}_1+\mathbf{r}) = \frac{dN(\mathbf{r}_1+\mathbf{r}|\mathbf{r}_1)}{\rho(\mathbf{r}_1+\mathbf{r})dS} \ , \tag{3}$$

where $dN(\mathbf{r}_1+\mathbf{r}|\mathbf{r}_1)$ is the average number of pairs in the surface element dS centered in $(\mathbf{r}_1+\mathbf{r})$ when one adatom is present at $\mathbf{r}_1$. For simplicity, we replace $\rho(\mathbf{r}_1+\mathbf{r})$ by an average density $\bar{\rho}$ independent of position. Since $g(r)$ is mainly used to characterize the intracluster, short-range correlation of the adatoms we chose $\bar{\rho}$ equal to the equilibrium density $\rho_c(\Theta,T)$ of the condensed phase, computed and discussed in Sec. IV. This choice implies that the long-range limit of $g(r)$ is Θ instead of 1.[36] Again for simplicity, in the following we display the planar and angular average $g(r)$ of $g(\mathbf{r}_1,\mathbf{r}_1+\mathbf{r})$.

Unless otherwise specified, all the time-dependent quantities have been computed for several temperatures and coverages as running averages over time slices of 0.2 nsec, short compared to the total simulation time, and long enough to provide a description of the system not too affected by random fluctuations.

The diffusion of the clusters has been computed for few sizes only, because the time scale for diffusion rapidly increases for sizes in excess of a few atoms.

The intracluster dynamics is characterized by the diffusion coefficient with respect to the cluster center of mass (CM). The inhomogeneity and anisotropy of the system suggest a separation of D into a tangential (D_t) and radial (D_r) components with respect to the CM direction. We shall also monitor the different diffusional behavior for atoms close to the CM and at the boundary of the clusters. Other quantities will be defined and displayed in the following sections.

III. THE SHORT-TIME AGGREGATION PROCESS

At the beginning of each simulation we randomly distribute the Ag adatoms on the C adsorption sites of the (111) Pt surface [see Fig. 1(a)], with the constraint that at most one atom can land on a given site.[37]

The number of adatoms corresponds to coverages $\Theta=0.10$, 0.25, 0.30. The strength of the Langevin white noise [Eq. (7)] has been set to study the system at $T=600$, 800, 1000 K. Few runs at $T=400$ K have also been performed.

A short time of the order of 10 ps, is sufficient to equilibrate the system at the target temperature. During this time, the system dynamics is influenced by the Langevin friction and white noise, and, therefore, cannot be considered as a very reliable description of the physical dynamics. Within the equilibration stage the atoms do not move much, the largest displacement being 15 Å at $\Theta=0.25$, $T=1000$ K, corresponding to few nearest-neighbor distances. This small displacement, however, is already able to modify the atomic configuration in a visible way, and to establish the first elements of order [See Fig. 1(b)]. We identify this first aggregation of atoms with nucleation.

To define the nucleation time τ_N in a quantitative way, we monitor the number $\mathcal{N}$ of clusters whose size is larger that a cutoff $\bar{N}$, corresponding to the smallest stable nu-

cleus (we took $\bar{N}=3$ for $\Theta=0.10$, and $\bar{N}=4$ for $\Theta=0.25$). Starting from deposition, $\mathcal{N}$ rapidly grows with time as nucleation takes place, and reaches a maximum. Then, very slowly, it decreases as the island's growth reduces the total number of aggregates on the surface. Our nucleation time τ_N is defined as the time at which $\mathcal{N}$ reaches the maximum, and is reported in Table I as a function of Θ and T.

With the beginning of nucleation within the time τ_N, the adatom-adatom interaction sets in, and our MD becomes more reliable in describing the real time dynamics of the system. Snapshots of the atomic configuration at regular intervals of time, reported in Fig. 1, show a clear tendency of the clusters to grow, and to form randomly connected islands, exchanging atoms with a dilute vapor.

On the time scale of the simulation, the aggregation process does not continue to produce a single, large, and stable island. Instead, the cluster formation process reaches a state of dynamical equilibrium, in which the condensation is compensated by evaporation of adatoms and small clusters, and also by the breaking of large aggregates into two or more almost equivalent parts of irregular shape. This is reflected in the time evolution of $P(N)$ (discussed below), that is rapid at the beginning of the simulation and reduces to thermal fluctuations within few nsec. The time τ_e after which we do not detect further systematic evolution of $P(N)$ is reported in Table I as a function of Θ and T.

As shown in Fig. 2, the adatoms, display a high diffusion rate, that does not change in time, and, in particular, does not vanish at τ_e. The simultaneous observation of a stationary distribution and of a fast diffusion of the adatoms (implying an efficient exchange of atoms and energy between the islands and the vapor) confirms that islands are in local, dynamical equilibrium with the vapor, that persist over times much longer than our simulation. We therefore identify τ_e with the end of the short-time aggregation process.

Of course, even our longest simulation cannot describe the system evolution over mesoscopic ($\sim\mu$sec) or macroscopic times, during which larger scale aggregation could take place either by cluster-cluster collision (coalescence) or indirect interaction via the vapor (Ostwald ripening).[11] Over this longer time scales, however, other phenomena will take place, involving defects, steps, etc., not fully taken into account in our study. This issue is further discussed in Sec. V.

A quantitative description of the nucleation and growth process is contained in the time dependence of the probability distribution $P(N)$, defined in Sec. II and

TABLE I. Temperature and coverage dependence of the nucleation time τ_N and early stage growth time τ_e.

	τ_N psec		τ_e psec	
T (K)	$\Theta=0.10$	$\Theta=0.25$	$\Theta=0.10$	$\Theta=0.25$
400	9.1	6.3	4550	3136
600	10.5	4.9	2240	1568
800	9.8	7.0	1383	1176
1000	10.5	5.6	1071	784

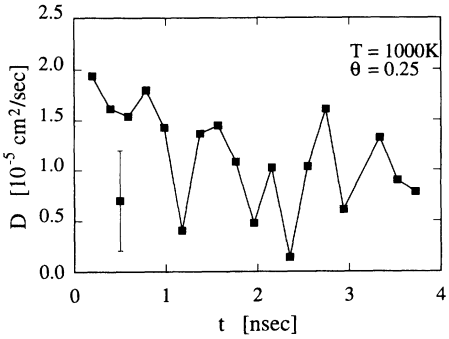

FIG. 2. Time dependence of the diffusion coefficient D_a of single adatoms, $\Theta=0.25$, $T=1000$ K. D_a is estimated from the adatom diffusion during 0.2 nsec. A typical error bar is indicated on the left.

displayed in Fig. 3, again for $\Theta=0.25$ and $T=1000$ K. The initial distribution [Fig. 3(a)] is approximately Gaussian, reflecting the random deposition process. After a very short time, $P(N)$ extends its range to larger sizes [Fig. 3(b) and 3(c)]. Within ~ 1 nsec $P(N)$ reaches a stationary distribution [Fig. 3 (d)]: the majority of the atoms belong to large aggregates with $N \geq 30$ [see also Fig. 4 displaying $p(N)$]; a small N population, however, never disappears, and gives rise to a nearly Gaussian distribution close to the origin of $P(N)$. A long and weak tail at higher sizes [apparent as a peak in $p(N)$, Fig. 4] is also present in our data, and corresponds to the occasional formation of metastable, large islands (N up to 100).

Of course, the large N portion of $P(N)$ is influenced by the finite simulation size and, therefore, should be interpreted with some caution. However, we argue that the results described in this section provide a reliable description of the system behavior on the nsec scale, since during this time the atomic average diffusion does not exceed

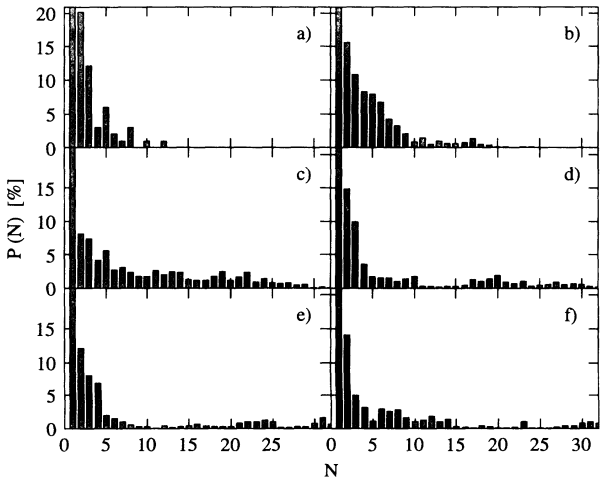

FIG. 3. Cluster size distribution $P(N)$ as a function of time, $\Theta=0.25$, $T=1000$ K. (a) Starting (random) distribution; (b) $t=\tau_N=5.6$ psec after deposition; (c) $t=0.4$ nsec; (d) $t=1.2$ nsec; (e) $t=2$ nsec; (f) $t=3$ nsec.

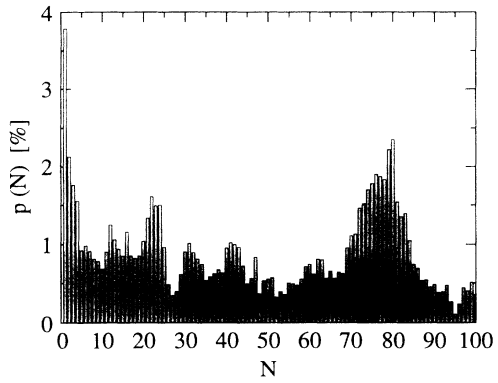

FIG. 4. Adatom probability $p(N)$ to belong to a cluster of size N, $\Theta=0.25$, $T=1000$ K, $t=3$ nsec after deposition.

the simulation cell size, and periodic boundary conditions do not influence the system evolution in a significant way.

The cluster condensation is reflected in the time evolution of the radial distribution function, reported in Fig. 5. Starting from the pair distribution function of a random deposition, the relaxation over the time τ_N starts to build the structure of $g(r)$ [see Fig. 5(a)], that fully develops after the ~ 1 nsec corresponding to τ_e [Fig. 5(b)]. Beyond that time no visible change occurs in $g(r)$.

At each stage of our simulation, the Ag adatoms remain strictly bound to the first overlayer plane, without any tendency to form 3D structures. Moreover, despite the large mismatch between Ag and Pt, despite the small lateral barriers, and in agreement with experiment, the density $\rho(\mathbf{R})$ is in registry with the potential corrugation, implying a large 2D compressibility of the adsorbed layer.

The global picture of the clustering process, here described for $\Theta=0.25$, $T=1000$ K, remains valid for the other coverages analyzed ($\Theta=0.10$, 0.30), with, however,

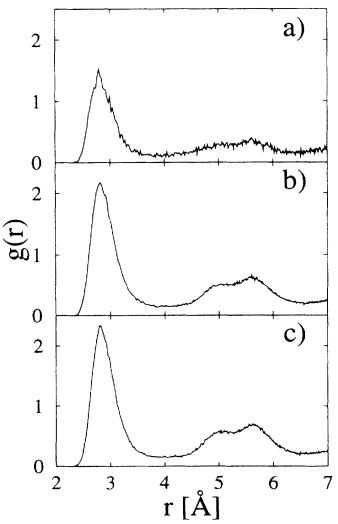

FIG. 5. Time dependence of the radial distribution function, $\Theta=0.25$, $T=1000$ K. (a) $t=\tau_N=5.6$ psec; (b) $t=0.7$ nsec; (c) $t=3.8$ nsec.

some specific features. First of all, nucleation and equilibration times monotonically decrease with increasing coverage, as the adatom-adatom interaction becomes stronger. Also expected and observed is a shift of the range of $P(N)$ toward larger sizes as Θ increases. Finally, starting from $\Theta=0.30$, clusters percolating across the entire simulation cell begin to appear, thus drastically modifying the physical process of equilibration.

The $\Theta=0.75$ case is, of course, well beyond this line, and will be discussed separately below.

More important and subtle are the changes induced by a lower equilibrium temperature. An oversimplified analysis would suggest an exponential increase of the characteristic times for nucleation and growth with decreasing T. The actual picture is more complex, since the different processes leading to thermodynamic equilibrium have significantly different activation energies, that, moreover, may depend on T in nontrivial ways.

The initial nucleation, for instance, requires mainly the diffusion of single adatoms or dimers. This process is virtually barrierless,[26] and therefore unaffected by temperature changes, at least for $T>400$ K. The processes contributing to growth, instead, have sizable activation barriers, and depend strongly on T. The evaporation of an atom from a cluster, for instance, requires at least 0.3 eV for clusters beyond $N\sim 10$. The activation barrier for cluster diffusion rapidly grows with size ($E_0=0.06$ eV for $N=1$, 0.09 eV for $N=2$, and 0.15 eV for $N=3$, from a simulation of the unfrozen interface, Ref. 26).

As a result, for each T we observe the nucleation of small clusters (up to about 10 atoms) within a time of the order of the picosecond, and almost independent of T. Only at the highest T we were able to unambiguously see equilibration by MD. At $T=800$ K the system is able to reach a stationary state within $\tau_e\sim 1.2$ nsec. At $T=600$ K τ_e is already roughly doubled, and some residual drift in $P(N)$ could be guessed beyond this time. At $T=400$ K, finally, the system is effectively frozen after the initial nucleation, and the time τ_e reported in Table I is only an estimate. Of course, the cutoff temperature for the occurrence of the different stages depend on the observation time. However, given the current estimates for the activation barriers of the aggregation process, we expect that the global picture emerging from our computation remains valid for the experimental systems, with, possibly, a quantitative difference in the cutoff temperature of ~ 100 K, and in the size of the observed clusters.

The progressive freezing of the system into a metastable configuration as T is decreased is reflected in the time dependence of the diffusion coefficient D (averaged over all the atoms in the adlayer). At all temperatures, diffusion is sizable at the beginning of the simulation, when adatoms travel over several interatomic distances to give rise to nucleation. At the highest T this high diffusion is only moderately reduced after ~ 1 nsec, while at low T the diffusion coefficient D drops by nearly two orders of magnitude to a residual value corresponding to intracluster diffusion only (see Fig. 6).

A similar information on the system dynamics could be inferred from the radial distribution functions. Starting at each temperature from the same random distribution,

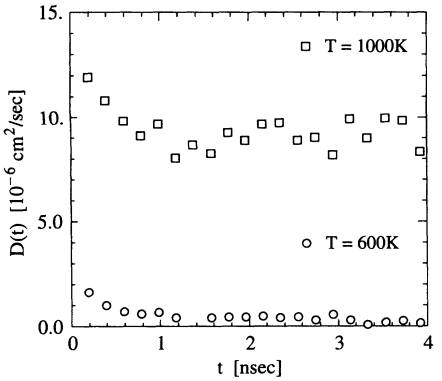

FIG. 6. Time dependence of the diffusion coefficient D, $\Theta=0.25$.

at low T the $g(r)$ soon develops deep minima among the peaks, almost vanishing between the first and second one. The presence of these "forbidden" interatomic distances clearly shows that atoms are almost unable to change their relative distance after a short initial time.

The highest coverage we analyzed was $\Theta=0.75$. The aim of this computation was to verify whether there is any symmetry between the $\Theta=0.25$ coverage and this system, having a 25% population of vacancies. The first requirement to observe this symmetry, of course, is that vacancies are stable and well recognizable entities. This is far from obvious in our system, where atomic positions are not rigidly constrained by the surface corrugation or adatom interaction, and whose behavior is very different from that of a lattice-gas model.

At high T ($T=1000$ K), in fact, we observe that the system is still in the two phases region, i.e., it is not homogeneous, and "bubbles" of empty surface are apparent. Voids, however, are not easily and not always recognizable as vacancies, or vacancy clusters [see Fig. 7(a)]. At $T=800$ K the adatom configuration is more regular, and the subdivision of the surface into the overlayer and the vacancy islands is more clear. Finally, at $T=600$ K this decomposition is apparent [Fig. 7(b)], and it is, therefore, meaningful to investigate the symmetry mentioned above. The first result concerns the dynamics of the islands formation. While it is difficult to distinguish the nucleation of vacancies for $\Theta=0.75$, it is apparent from snapshots that the early stage aggregation proceeds faster for this high coverage than in the corresponding $\Theta=0.25$ case. It is also apparent that the density of single advacancies (i.e., the vapor in the vacancy picture) has a higher density than the adatom density for $\Theta=0.25$. These two observations, of course, imply that there is no strict and quantitative symmetry between the two systems. Moreover, we observe that island's dimensions are smaller for the vacancies than for the adatoms, and also the shapes are rather different, since the boundary of vacancy's islands is usually smoother and better defined than those of adclusters.

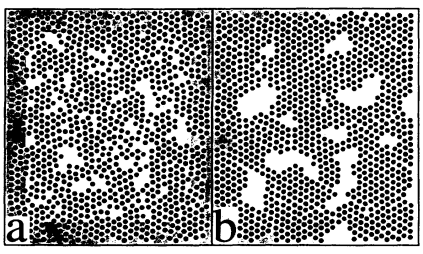

FIG. 7. Snapshots of atomic configurations, $\Theta=0.75$, $T=1000$ K (left), and $T=600$ K (right), $t>\tau_e$.

IV. THE EQUILIBRIUM PROPERTIES

The short time required by the system to reach a stationary configuration allows a detailed analysis of the properties of the resulting phases for the adsorbed overlayer. These are either equilibrium phases at high T ($T\geq 600$ K), or metastable phases at lower T.

The cluster aggregation we described in Sec. III is obviously the consequence of the fact that an homogeneous distribution of adatoms is unstable under the (Θ, T) conditions of our study. Instead, our systems are in the two phases coexistence region of the phase diagram and the clusters are samples of the "condensed" phase in equilibrium with a dilute vapor. In the following, we consider single adatoms and dimers as vapor, and all the clusters with $N>2$ as condensate. Of course, this definition is arbitrary, but the resulting analysis does not depend much on the choice of this boundary.

The first property we want to discuss is the density of the two phases as a function of Θ and T. Given the inhomogeneous nature of the system, and the irregular cluster boundaries, we lack a unique definition of cluster area or density. We apply the following operational definition, devised to measure the excluded surface associated with each cluster: the entire surface is partitioned into triangles, each having an adsorption site C or A at his center (center of mass of the triangle ζ). Each atom i in a cluster occupies entirely the triangle if $\mathbf{R}_i$ is within the triangle. Moreover, it occupies $\frac{1}{3}$ of all the triangles whose distance $|\mathbf{R}_i-\zeta|$ are within a cutoff distance $\Re$. The cut off distance $\Re$ has been chosen equal to the excluded radius in the radial distribution function, corresponding to ~ 2 occupied triangles per atom. The cluster area is the sum of all the surfaces occupied by its atoms. We verified that this definition of the cluster surface reduces to the intuitive one for regular atomic configuration. Even if we do not assume any coverage or T dependence in $\Re$, the cluster surface acquires a dependence by the fact that disorder causes atoms to occupy, from time to time, more than two triangles.

In principle, the intracluster density defined above is dependent not only on Θ and T, but also on N. The main effect we expect is due to the surface-tension pressure, more important for small clusters than for larger ones. However, we are unable to measure this last dependence outside the error bar of our computation, and therefore, we report in Fig. 8 the average value for clusters of size $N>10$.

The area occupied by the vapor is defined as the difference between the total area and the area occupied by all the clusters with $N>2$. The corresponding vapor

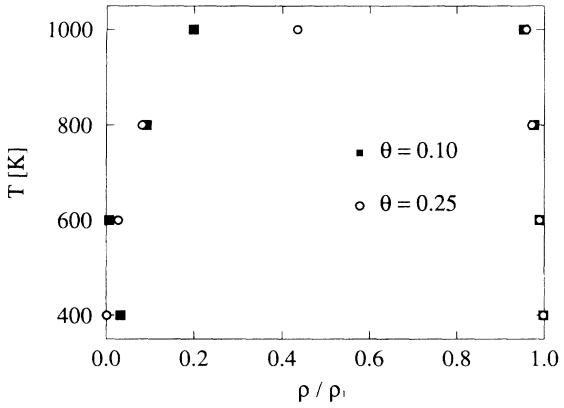

FIG. 8. Vapor-condensate coexistence curve. Dots denote $\Theta=0.25$; squares denote $\Theta=0.10$. ρ_1 is the density of a filled monolayer.

density is also reported in Fig. 8. At low T most of this density is due to single adatoms. At $T=1000$ K and $\Theta=0.25$, instead, the dimer contribution starts to become substantial. The $\rho(T)$ curve has the usual bell shape of the liquid-vapor coexistence, and already from the limited temperature range of our simulation is possible to appreciate the thermal expansion of the islands and the increasing vapor tension with increasing T. The liquid and vapor branches of the curve will join at a "critical temperature" T_c, that, however, we are unable to explore since it is well beyond the desorption temperature for Ag/Pt(111). The figure clearly shows that the coexistence curve is asymmetric with respect to the critical point, this being consistent with the asymmetry of adatoms and advacancies discussed in Sec. III.[5]

The first characterization of the "equilibrium" island population is in terms of the cluster size distribution, already introduced in Sec. III to describe the system evolution up to τ_e. The results for the long-time averages (average time of the order of few nsec, starting from t well beyond τ_e) are summarized in Fig. 9, displaying the equilibrium $P(N)$ as a function of Θ and T. Two trends are apparent.

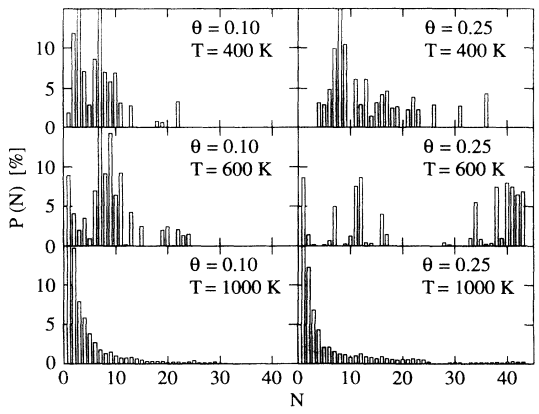

FIG. 9. Coverage and T dependence of $P(N)$, $t > \tau_e$.

(i) As expected, $P(N)$ shifts toward larger aggregates with increasing Θ.

(ii) The effect of temperature is nonmonotonic: decreasing T in the range 1000–800 K favors larger clusters. Below this temperature, the slowing of the cluster growth beyond τ_N prevails, and $P(N)$ is again shifted to smaller sizes.

An easy analysis of cluster energetics in terms of bond numbers suggests an enhanced stability for a series of compact two-dimensional structures $N=7$, 10, etc.,[38]). This special stability, in turn, should be reflected in peaks of $P(N)$. Examination of Fig. 9, however, shows that little structure is recognizable in $P(N)$. At high T, in fact, $P(N)$ is smooth and regular, without special features at $N=7$ or 10. At lower T ($T=800$ K) more structure begin to appear in $P(N)$, and it is possible to single out some sizes as specially stable: $N=7$ is apparent, $N=10$ can be guessed. However, down to the temperatures we are able to simulate, even these sizes do not represent dominant features in $P(N)$. Moreover, the clusters corresponding to the "magic sizes" often display a shape different from that expected on the basis of bonds counting arguments. The conclusion, of course, could be different at even lower T, for which the energy considerations become dominant, as opposed to the entropic contributions apparently more relevant at the T of our study.

The importance of entropy and dynamics is highlighted by the analysis of cluster shapes and local order. Snapshots of atomic configurations immediately show that down to the lowest T of our study the islands are far from static, as shown in Fig. 10 displaying the shape transformations undergone by a cluster at $T=400$ K, $\Theta=0.25$. A synthetic description of the island's shape is provided by the ratio r between the smallest and the largest of the 2D moments of inertia. At each T and Θ, $r(N)$ is well below 1 for every N, making apparent the preference of the system for irregular shapes. In particular, there is no peak in r at the "magic numbers." Fluctuations of r in time are large, underlying the fast shape changes, and the frequent appearance of elongated structures leading to fragmentation.

Because of these fluctuations it is difficult to recognize a clear trend of $r(N)$ with T. A gross analysis suggests that also $r(N)$ is nonmonotonic with T. At low T (below 600 K) r is reduced by the long persistence of metastable elongated structures. At higher T (around 800 K) these

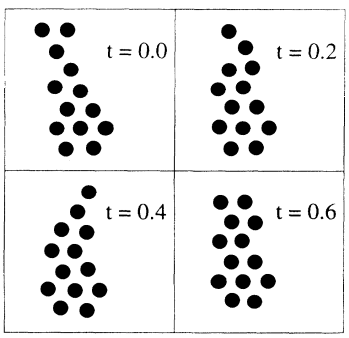

FIG. 10. Snapshots of atomic configurations for a cluster, $\Theta=0.25$, $T=400$ K; the snapshots are separated by 0.2 nsec.

structure readily rearrange into more compact clusters, and $r(N)$ slightly increases. Beyond this T thermal disorder prevails, and r decreases again.

The sequence in Fig. 10 highlights an important feature of the cluster dynamics: at moderate T it is often possible to recognize a compact and ordered core inside the cluster (the regular heptamer in Fig. 10) that does not change in time. The core is surrounded by less tightly bound and far more mobile atoms producing the rapid shape changes. This observation can be quantified by computing the diffusion coefficient for atoms at the center and at the boundary of large clusters, clearly showing the enhanced mobility at the boundary. This computation also shows that diffusion occurs mainly tangentially ($D_t \gg D_r$), with limited exchange of atoms between the core and the boundary. The intracluster diffusion produces a slow, amoebalike migration of the entire cluster. For $N=36$ the diffusion coefficient of the cluster CM is roughly two orders of magnitude smaller that for the single adatoms.

In large clusters (beyond ~ 15 atoms) the shape changes are accompanied by the appearance of structural defects (vacancies, dislocations, etc.) whose frequency rapidly increases with T, and eventually destroys the local atomic order. A detailed analysis of many atomic configurations suggests the following classifications of the "state" of the islands as a function of T: (i) at low T (below ~ 600 K) the local atomic order is always apparent, despite the global shape changes. (ii) At intermediate T (between 600 and 800 K) the clusters tend to display an ordered core surrounded by a liquidlike boundary. (iii) At higher T the islands are clearly liquidlike. These different "states" are exemplified in Fig. 11.

The structural evolution with T is reflected in the radial distribution function of the adatoms, whose Θ and T dependence is displayed in Fig. 12. At all the Θ and T of our simulation the most notable features of $g(r)$ are the high first peak, the deep minimum beyond it, and a double humped second peak, including both the second and third-nearest-neighbor shells. All of these features are strongly influenced by the surface corrugation and by the 2D character of the system, enhancing the oscillations of $g(r)$. Despite this strong modulation, the $g(r)$ at $T=1000$ K is clearly liquidlike, with a first peak extending over more than 1.5 Å. The minima in $g(r)$ between the peaks become deeper and wider at $T=800$ K, and almost vanish at $T \leq 600$ K. At these moderate T the computed $g(r)$ clearly display the characteristic features due to quenched disorder usually observed in amorphous system, here induced by the presence of an external potential not commensurate with the natural periodicity of the adatoms.

To evaluate the importance of the surface corrugation, and, in particular, of the strain induced by the Pt substrate on the Ag overlayer, we performed a series of computations with a simplified model in which both the Φ_{PtAg} potential and the ρ^{PtAg} electron density were averaged along the xy plane.

We started the new simulation from the well equilibrated output configurations at $\Theta=0.25$, $T=400$, 800, 1000 K, all displaying a population of dynamically stable islands. As expected, the first effect of removing the substrate corrugation is an expansion of the Ag-Ag interatomic distance to match that of bulk Ag. Over longer times, a systematic trend becomes apparent, as the fragmented islands collapse in a unique, compact aggregate again surrounded by a vapor of adatoms. The process is comparatively faster at lower temperature, as the driving force (free energy excess) toward a single condensed domain becomes stronger. Only at the highest simulated temperature ($T=1000$ K) the thermal motion starts to prevail, and fragments again the single aggregate in a population of islands of various sizes.

Our study confirms that strain plays an important role in determining the cluster size distribution. Special care, however, is required in comparing our simulation with the experimental results in Ref. 14, since the two studies analyze the system properties over drastically different

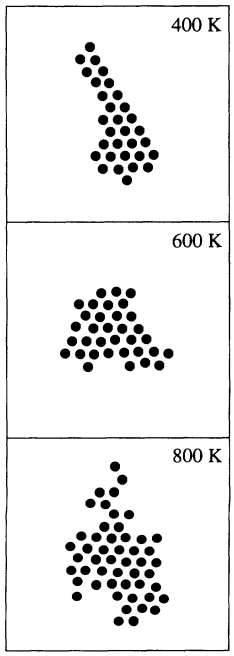

FIG. 11. Snapshots of atomic configurations exemplifying the three phases observed in the simulation (see text), $\Theta=0.25$.

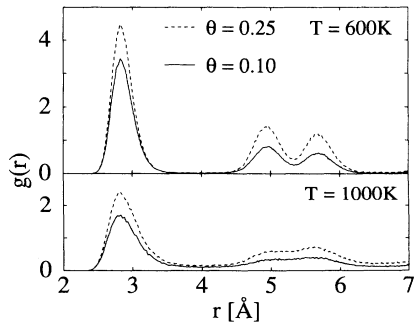

FIG. 12. Dependence on Θ and T of the radial distribution function. The averages have been collected after the early stage growth.

time scales. In particular, over the macroscopic observation times of the experiment, the Ag-Pt mixing, excluded in our model, may become the dominant feature in the interface morphology.[16] A detailed discussion, including the comparison with the strain free Pt/Pt(111) interface, is reported in Ref. 39.

V. STEPS ON THE Pt(111) SURFACE

The main qualitative feature of experimental systems missing in the model described above is the interaction of the adatoms with the surface defects and especially with steps. Experiments clearly show that steps, always present even on the most compact and stable surfaces, act as sinks for the adsorbed species. Following deposition, adatoms and clusters will migrate on terraces, until when they reach a step. There adatoms increase their coordination, and, therefore, experience an attractive potential that, at moderate T, confines their movement. Eventually, some of the adatoms will find a way to cross the step, and to slowly migrate inside the upper terrace.[16]

To investigate the effect of steps on the nucleation and growth of islands on the Ag/Pt(111) interface we created two opposite steps on our surface by removing 29 rows of Pt atoms of the uppermost plane. It is easy to verify that two parallel steps along the principal directions of the (111) surface cannot be equivalent, but differ in the relative position of the edge atoms and the second substrate layer. Despite this small difference, we prefer the simplicity of this configuration over more complex geometries involving only one kind of step. We relaxed the Pt surface before the Ag deposition, and again we froze the substrate (but not the upper Pt terrace).

The major aim of this computation is to analyze how the influence of the steps propagates in time and distance upon random deposition of Ag atoms, thus providing an estimate of the validity range for our previous analysis of adsorbates on terraces. The frozen substrate approximation prevents the investigation of the diffusion of adatoms into the terraces. This, however, is a slow process compared to the nucleation and growth, and does not significantly affect these phenomena.[40]

Our simulation has been performed at $\Theta=0.25$ and $T=1000$ K. The first indication of the effect of steps on the adsorbate distribution is obtained from a plot of $P_{\mathrm{Ag}}(x)$, where x is the direction perpendicular to the steps (see Fig. 13). The nucleation time $\tau_N=\sim 6$ psec is already sufficient to create a clear density peak in the first row of the lower terrace adjacent to the steps. After ~ 0.4 nsec the first row is almost filled by adatoms, and a peak starts to develop on the following row. This process of filling and then propagation of the perturbation to the next row (wetting) proceeds at a regular rate, with one added row every ~ 0.4 nsec. The process is limited by adatom diffusion in the rectangular region (roughly three row wide) adjacent to the growing step, that appears depleted of adatoms.

In the presence of a constant flow of adatoms, the steps will move to close the lower terrace, until when a new layer will start to grow. In the condition of the present simulation at constant number of adatoms, the process terminates when all the Ag is adsorbed at the steps, with only a residual distribution of adatoms rapidly diffusing in between.

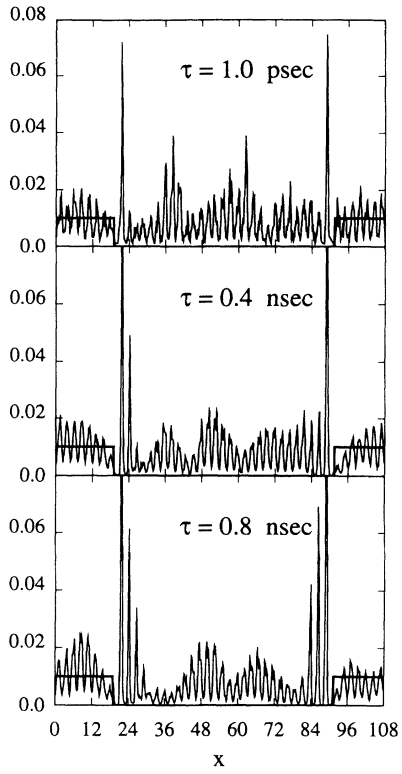

FIG. 13. Adatom distribution probability $P(x)$ along the direction perpendicular to the steps, $\Theta=0.25$, $T=1000$ K.

The upper terrace appears to be much less affected than the lower one, apparently because the effective potential is weaker and slightly repulsive on this side of the step. Over times of the order of 3 nsec, in fact, the evolution of adatoms and clusters in the upper terrace is similar to that described in the previous sections. Only beyond this time the effect of the steps manifest itself also in the upper terrace configuration. At $\tau=\sim 4$ nsec the step repulsive potential (together with the small size of our system) confines the adatoms at the center of the upper terrace in a unique large islands surrounded by the vapor.

These observations set the limit for our description of the previous sections for the experimental systems. Up to ~ 1 nsec (i.e., comparable to the early stage growth time) the effect of the steps extends over few atomic rows in the lower terrace only. For terrace widths of the order of 1000 Å, therefore, our study of the ideal surface remains valid for most of the system during times longer than the early stage growth and extending well into the late stage aggregation.

Over times exceeding ~ 50 nsec the effect of the steps extends over most of the surface, and a realistic model has to take into account their presence to quantitatively describe the system evolution.

The times reported and discussed in this section all refer to the $\Theta=0.25$, $T=1000$ K case, and we expect

only a moderate dependence on Θ. For different temperatures, instead, these times must be rescaled, for instance, by using the temperature dependence of τ_e as a guideline.

VI. CONCLUSIONS

By MD in the EAM framework we have simulated the nucleation and early stage growth of a Ag submonolayer ($\Theta=0.10$, 0.25, 0.30, and 0.75) on the Pt (111) surface for temperatures ranging from 400 to 1000 K. We have computed and discussed the time evolution of the cluster size distribution and shape, of the diffusion coefficient, and of the radial distribution function.

For the higher temperatures ($T>600$ K) we have analyzed the properties of the Ag islands in local equilibrium with the vapor of Ag adatoms.

Finally, we have studied the effect of steps on the system evolution and equilibrium properties.

In this last section we would like to summarize few considerations relevant to assess the validity of the present study in describing the experimental systems.

First of all, let us remind you that the Ag and Pt are both metals with filled or nearly filled d bands, and, as such, are reliably described by the EAM. Moreover, experimental evidence shows that Ag in Ag/Pt(111) always displays an electronic structure similar to that of bulk,[13] suggesting that the validity of the EAM description extends to this inhomogeneous system.

Our MD computation covers very long times, reaching ~ 10 nsec at the lower coverages. We are, therefore, able to fully describe nucleation, and, at least at $T>600$ K the early stage growth. The size of the system (930 atoms per surface plane) guarantees that over the time scale of our simulation the results are unaffected by the periodic boundary conditions.

Concerning the main limitations of our computation, we mention that EAM has quantitative problems in describing surface energies, and that the diffusion coefficient predicted by the present model for a single adatom on the (111) surface could be somewhat lower than the experimental value. It is not obvious, however, that this deficiencies will affect the relevant features of our results. At coverages $\Theta \geq 0.10$ the adatom motion is much more dependent on the adatom-adatom interaction than on the interaction with the substrate. Moreover, during all the simulation we explore a limited region of the configuration space. In particular, our atoms rarely experience changes in the coordination comparable to those involved in the formation of a new surface. We therefore expect that, over these restricted conditions, EAM reliably describes forces and, therefore, the dynamics of our system.

Our investigation has been performed at constant number of adatoms on the surface. It is, therefore, natural to wonder what are the changes induced by a steady flow of adatoms, that is the condition of most experiments. We observe that normal deposition rates require macroscopic times to form one layer, and therefore, addition of even a single adatom to the simulated surface would be very unlikely during the time of our computation.

Finally, we underline that we have performed a limited investigation of the effect of steps on the system evolution. This study confirms the relevance of our description for the nucleation and early stage growth of Ag on high quality Pt(111) surfaces.

This specific feature, i.e., interaction of adatoms with steps and other surface defects, is the major improvement required for a fully quantitative description of the system evolution over mesoscopic and macroscopic times. This investigation requires methods different from MD, that, however, will still be useful to provide key quantities entering phenomenological equations, and to test the short-time prediction of dynamical theories.

ACKNOWLEDGMENTS

This work has been partially supported by the Swiss National Science Foundation under Grants Nos. 20-5446.87 (P. Blandin), and 20-31240.91 (C. Massobrio).

[1]See, for instance, Proceedings of the Twelfth International Vacuum Congress, The Hague, 1992, edited by A. W. Klein [Surf. Sci. **287/288** (1993); Appl. Surf. Sci. **70/71** (1993)]; *Kinetics of Ordering and Growth at Surfaces,* edited by M. G. Lagally (Plenum, New York, 1990).

[2]See, for instance, *Electronic Structure of Metal-Semiconductor Contacts,* edited by W. Mönch (Kluwer Academic, Dordrecht, 1990).

[3]*Handbook of Thin Film Deposition Processes and Techniques,* edited by K. K. Schuegraf (Noyes Publications, Park Ridge, New Jersey, 1988); *Atomic Layer Growth and Processing,* edited by T. F. Kuech, P. D. Dapkus, and Y. Aoyagi, MRS Symposia Proceedings No. 222 (Materials Research Society, Pittsburgh, 1991).

[4]C. Argile and G. E. Rhead, Surf. Sci. Rep. **10**, 277 (1989).

[5]B. N. J. Persson, Surf. Sci. Rep. **15**, 1 (1992).

[6]W. D. Luedtke and U. Landman, Phys. Rev. B **44**, 5970 (1991); T. J. Raeker and A. E. DePristo, J. Vac. Sci. Technol A **10**, 2396 (1992).

[7]K. Binder and D. Stauffer, Adv. Phys. **25**, 343 (1976).

[8]J. W. Cahn and J. E. Hilliard, J. Chem. Phys. **28**, 258 (1958); **31**, 688 (1959).

[9]A. Zangwill, *Physics at Surfaces* (Cambridge University Press, Cambridge, 1988).

[10]J. A. Venables, Philos. Mag. **27**, 697 (1973).

[11]M. Zinke-Allmang, L. C. Feldman, and M. H. Grabow, Surf. Sci. Rep. **16**, 377 (1992).

[12]P. W. Davies, M. A. Quinlan, and G. A. Samorjai, Surf. Sci. **121**, 290 (1982).

[13]B. Schmiedeskamp *et al.,* Surf. Sci. **223**, 465 (1989).

[14]A. F. Becker, G. Rosenfeld, B. Poelsema, and G. Comsa, Phys. Rev. Lett. **70**, 477 (1993).

[15]The Härtel, U. Strüber, and J. Küppers, Thin Solid Films **229**, 163 (1993); U. Strüber and J. Küppers, Surf. Sci. Lett. **294**,

L924 (1993).
[16]H. Röder, R. Schuster, H. Brune, and K. Kern, Phys. Rev. Lett. **71**, 2086 (1993).
[17]A. R. Sandy *et al.*, Phys. Rev. Lett. **68**, 2192 (1992); G. Grübel *et al.*, Phys. Rev. B **48**, 18 119 (1993).
[18]R. J. Behm, in *Scanning Tunneling Microscopy and Related Methods,* of *NATO Advanced Study Institute, Series E,* edited by R. J. Behm, N. Garcia, and H. Rohrer (Kluwer Academic, New York, 1990).
[19]G. Lehmpfuhl and Y. Uchida, Surf. Sci. **235**, 295 (1990).
[20]See, A. E. Carlsson, Solid State Phys. **43**, 1 (1990), for a discussion of the EAM and closely related models.
[21]M. S. Daw and M. I. Baskes, Phys. Rev. **29**, 6443 (1984).
[22]M. S. Daw, and R. L. Hatcher, Solid State Commun. **56**, 697 (1985); S. M. Foiles, Phys. Rev. B **32**, 3409 (1985).
[23]S. M. Foiles, M. I. Baskes, and M. S. Daw, Phys. Rev. B **33**, 7983 (1986).
[24]M. S. Daw and S. M. Foiles, J. Vac. Sci. Technol. A **4**, 1412 (1986); M. S. Daw, Surf. Sci. **166**, L161 (1986); S. M. Foiles, *ibid.* **191**, L779 (1987).
[25]Chung-Li Liu and J. B. Adams, Surf. Sci. **294**, 211 (1993).
[26]P. Blandin and C. Massobrio, Surf. Sci. **279**, L219 (1992); C. Massobrio and P. Blandin, Phys. Rev. B **47**, 13 687 (1993).
[27]M. S. Daw, Phys. Rev. B **39**, 7441 (1989); T. J. Raeker and A. E. DePristo, *ibid.* **39**, 9967 (1989); M. I. Baskes, *ibid.* **46**, 2727 (1992); S. M. Foiles, *ibid.* **48**, 4287 (1993).
[28]W. R. Tyson and W. A. Miller, Surf. Sci. **62**, 267 (1977).
[29]D. Schumaker and D. Stark, Surf. Sci. **123**, 384 (1982), observe adatom diffusion at 78 K. The value for D_0 is estimated by C. Roth, Diplomarbeit, Universität Düsseldorf, Düsseldorf, 1989.
[30]J. P. Chauvineau, Surf. Sci. **93**, 471 (1980).
[31]H. Röder, H. Brune, J.-P. Bucher, and K. Kern, Surf. Sci. **298**, 121 (1993).
[32]We applied the algorithms described in R. Biswas and D. R. Hamann, Phys. Rev. B **34**, 895 (1986), to sample $\mathbf{F}_W$.
[33]For a flat surface D, γ, and F_W are trivially related.
[34]M. P. Allen and D. J. Tildesley, *Computer Simulation of Liquids* (Clarendon, Oxford, 1989).
[35]The snapshots of the atomic configurations are available from the authors.
[36]The alternative choice $\bar{\rho}=\langle\rho(\mathbf{r})\rangle$, giving the correct long-range limit of $g(r)$, would introduce a spurious dependence proportional to Θ^{-1} in the short-range part of $g(r)$.
[37]Our starting condition is reproduced in experiments in which atoms are adsorbed on a cold surface, and the system is then annealed at higher temperature.
[38]G. Rosenfeld *et al.*, Phys. Rev. Lett. **69**, 917 (1992); J. W. Norskov, K. W. Jacobsen, P. Stoltze, and L. B. Hansen, Surf. Sci. **283**, 277 (1993).
[39]P. Blandin, C. Massobrio, and P. Ballone (unpublished).
[40]Complete surface mixing takes $\sim 10^2$ sec at $T=650$ K (Ref. 16).

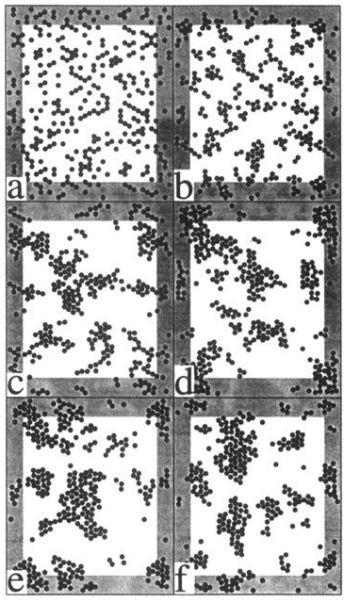

FIG. 1. Snapshots of the adatom configurations, $\Theta = 0.25$, $T = 1000$ K. (a) Starting (random) distribution; (b) $t = \tau_N = 5.6$ psec after deposition; (c) $t = 0.8$ nsec; (d) $t = 1.6$ nsec; (e) $t = 2.4$ nsec; (f) $t = 3.8$ nsec. The shaded area belongs to the periodic replicas of the central region.

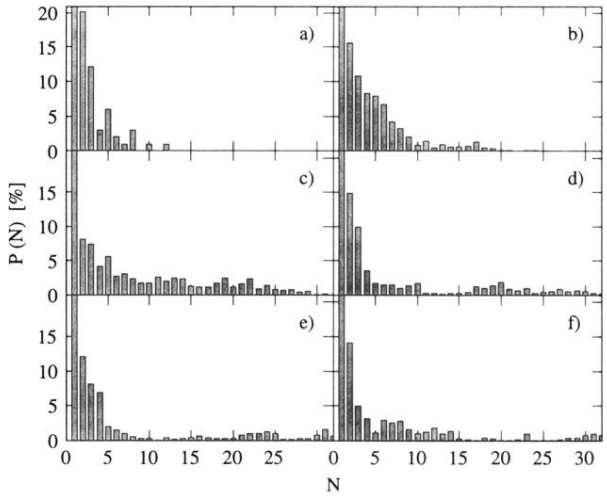

FIG. 3. Cluster size distribution $P(N)$ as a function of time, $\Theta=0.25$, $T=1000$ K. (a) Starting (random) distribution; (b) $t=\tau_N=5.6$ psec after deposition; (c) $t=0.4$ nsec; (d) $t=1.2$ nsec; (e) $t=2$ nsec; (f) $t=3$ nsec.

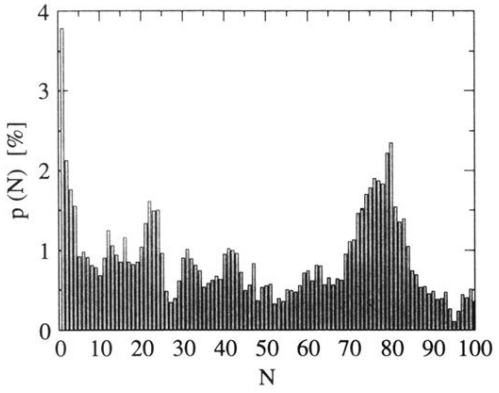

FIG. 4. Adatom probability $p(N)$ to belong to a cluster of size N, $\Theta = 0.25$, $T = 1000$ K, $t = 3$ nsec after deposition.

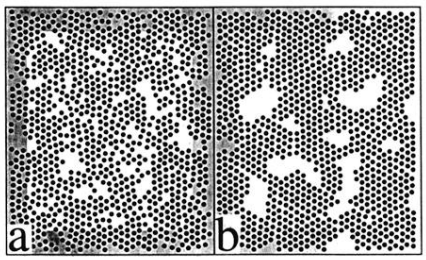

FIG. 7. Snapshots of atomic configurations, $\Theta = 0.75$, $T = 1000$ K (left), and $T = 600$ K (right), $t > \tau_e$.

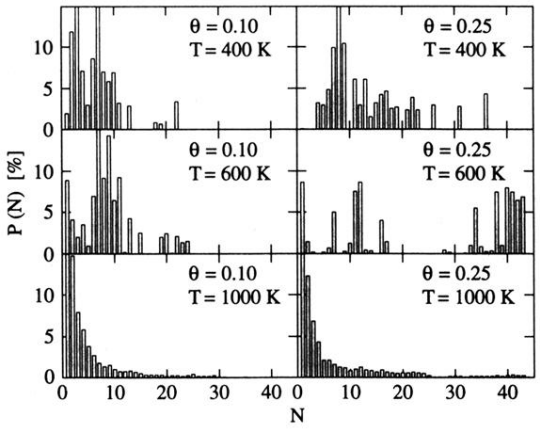

FIG. 9. Coverage and T dependence of $P(N)$, $t > \tau_e$.